Comparative Analysis of CFD Models of Dense Gas–Solid Systems

B. G. M. van Wachem, J. C. Schouten, and C. M. van den Bleek
DelftChemTech, Chemical Reactor Engineering Section, Delft University of Technology, 2628 BL Delft, The Netherlands

R. Krishna
Dept. of Chemical Engineering, University of Amsterdam, 1018 WV Amsterdam, The Netherlands

J. L. Sinclair
School of Chemical Engineering, Purdue University, West Lafayette, IN 47907

Many gas–solid CFD models have been put forth by academic researchers, government laboratories, and commercial vendors. These models often differ in terms of both the form of the governing equations and the closure relations, resulting in much confusion in the literature. These various forms in the literature and in commercial codes are reviewed and the resulting hydrodynamics through CFD simulations of fluidized beds compared. Experimental data on fluidized beds of Hilligardt and Werther (1986), Kehoe and Davidson (1971), Darton et al.(1977), and Kuipers (1990) are used to quantitatively assess the various treatments. Predictions based on the commonly used governing equations of Ishii (1975) do not differ from those of Anderson and Jackson (1967) in terms of macroscopic flow behavior, but differ on a local scale. Flow predictions are not sensitive to the use of different solid stress models or radial distribution functions, as different approaches are very similar in dense flow regimes. The application of a different drag model, however, significantly impacts the flow of the solids phase. A simplified algebraic granular energy-balance equation is proposed for determining the granular temperature, instead of solving the full granular energy balance. This simplification does not lead to significantly different results, but it does reduce the computational effort of the simulations by about 20%.

Introduction

Gas–solid systems are found in many operations in the chemical, petroleum, pharmaceutical, agricultural, biochemical, food, electronic, and power-generation industries. Computational fluid dynamics (CFD) is an emerging technique for predicting the flow behavior of these systems, as it is necessary for scale-up, design, or optimization. For example, Barthod et al. (1999) have successfully improved the performance of a fluidized bed in the petroleum industries by means of CFD calculations. Sinclair (1997) gives an extensive introduction on applying CFD models for gas/solid risers. Although single-phase flow CFD tools are now widely and successfully applied, multiphase CFD is still not because of the difficulty in describing the variety of interactions in these systems. For example, to date there is no agreement on the appropriate closure models. Furthermore, there is still no agreement on even the governing equations. In addition, proposed constitutive models for the solid-phase stresses and the interphase momentum transfer are partially empirical.

CFD models of gas–solid systems can be divided into two groups, Lagrangian models and Eulerian models. Lagrangian models, or discrete particle models, calculate the path and

Correspondence concerning this article should be addressed to B. G. M. van Wachem.
Current address for B. G. M. van Wachem and J. C. Schouten: Laboratory of Chemical Reactor Engineering, Eindhoven University of Technology, P. O. Box 513, 5600 MB Eindhoven, The Netherlands.

motion of each particle. The interactions between the particles are described by either a potential force (soft-particle dynamics, Tsuji et al., 1993) or by collision dynamics (hard-particle dynamics, Hoomans et al., 1995). The drawbacks of the Lagrangian approach are the large memory requirements and the long calculation time and, unless the continuous phase is described using direct numerical simulations (DNS), empirical data and correlations are required to describe the gas–solid interactions. Eulerian models treat the particle phase as a continuum and average out motion on the scale of individual particles, thus enabling computations by this method to treat dense-phase flows and systems of realistic size. As a result, CFD modeling based on this Eulerian framework is still the only feasible approach for performing parametric investigation and scale-up and design studies.

This article focuses on the Eulerian approach and compares the two sets of governing equations, the different closure models, and their associated parameters that are employed in the literature to predict the flow behavior of gas–solid systems. Unfortunately, many researchers propose governing equations without citing, or with incorrectly citing, a reference for the basis for their equations. Both Anderson and Jackson (1967) and Ishii (1975) have derived multiphase flow equations from first principles, but the inherent assumptions in these two sets of governing equations constrain the types of multiphase flows to which they can be applied. One of the objectives of our current contribution is to show how these two treatments differ; it is shown that Ishii's (1975) treatment is appropriate for a dispersed phase consisting of fluid droplets, and that Anderson and Jackson's (1967) treatment is appropriate for a dispersed phase consisting of solid particles. In the case of a solid dispersed phase, many researchers and commercial CFD codes employ kinetic theory concepts to describe the solid-phase stresses resulting from particle–particle interactions. Various forms of the constitutive models based on these concepts have been applied in the literature. The qualitative and quantitative differences between these are shown in this article. The predictions of CFD simulations of bubbling fluidized beds, slugging fluidized beds, and bubble injection into fluidized beds incorporating these various treatments are compared to the "benchmark" experimental data of Hilligardt and Werther (1986), Kehoe and Davidson (1971), Darton et al. (1977), and Kuipers (1990).

Governing Equations

Most authors who refer to the origin of their governing equations refer to the work of Anderson and Jackson (1967) or Ishii (1975). Anderson and Jackson (1967) and Jackson (1997) [with correction in Jackson (1998)] use a formal mathematical definition of local mean variables to translate the point Navier-Stokes equations for the fluid and the Newton's equation of motion for a single particle directly into continuum equations representing momentum balances for the fluid and solid phases, as earlier suggested by Jackson (1963). The point variables are averaged over regions that are large with respect to the particle diameter, but small with respect to the characteristic dimension of the complete system. A weighting function, $g(|x-y|)$, is introduced in forming the local averages of system point variables, where $|x-y|$ denotes the separation of two arbitrary points in space. The integral of g over the total space is normalized to unity:

$$4\pi\int_0^\infty g(r)r^2\,dr = 1. \tag{1}$$

The "radius" l of function g is defined by

$$\int_0^l g(r)r^2\,dr = \int_l^\infty g(r)r^2\,dr, \tag{2}$$

If l is chosen to satisfy $a \ll l \ll L$, where a is the particle radius and L is the shortest macroscopic length scale, averages defined should not depend significantly on the particular functional form of g or its radius.

The gas-phase volume-fraction $\epsilon(x)_g$ and the particle number density $n(x)$ at point x are directly related to the weighting function g:

$$\epsilon(x)_g = \int_{V_g} g(|x-y|)\,dV_y \tag{3}$$

$$n(x) = \sum_p g(|x-x_p|), \tag{4}$$

where V_g is the fluid-phase volume, and x_p is the position of the center of particle p. The local mean value of the fluid-phase point properties, $< f >_g$, is defined by

$$\epsilon(x)_g < f >_g(x) = \int_{V_g} f(y)\,g(|x-y|)\,dV_y. \tag{5}$$

The solid-phase averages are not defined like the fluid-phase averages, since the motion of the solid phase is determined with respect to the center of the particle, and average properties need only depend on the properties of the particle as a whole. Hence, the local mean value of the solid-phase point properties is defined by

$$n(x) < f >_s(x) = \sum_p f_s(|x-x_p|). \tag{6}$$

The average space and time derivatives for the fluid and solid phases follow from the preceding definitions. The averaging rules are then applied to the point continuity and momentum balances for the fluid. For the solid phase, the averaging rules are applied to the equation of motion of a single particle p:

$$\rho_s V_p \frac{\partial \boldsymbol{v}_s}{\partial t} = \int_{S_p} \bar{\bar{\sigma}}_g(y)\,n(y)\,ds_y + \sum_{q\neq p} f_{qp} + \rho_s V_p g, \tag{7}$$

where $\boldsymbol{v}_s$ is the particle velocity, ρ_s is the particle density, V_p is the volume of particle p, $\bar{\bar{\sigma}}_g$ is the gas-phase stress tensor, S_p denotes the surface of particle p, and f_{qp} represents the resultant force exerted on the particle p from contacts with other particles.

The resulting momentum balances for the fluid and solid phases, dropping the averaging brackets $< >$ on the vari-

ables, are as follows:

$$\rho_g \epsilon_g \left[\frac{\partial}{\partial t} \boldsymbol{v}_g + \boldsymbol{v}_g \cdot \nabla \boldsymbol{v}_g \right] = \nabla \left(\epsilon_g \bar{\bar{\sigma}}_g \right) - \sum_p \int_{S_p} \bar{\bar{\sigma}}_g \cdot n(y)\, g\, |x - y|\, ds_y + \rho_g \epsilon_g g \quad (8)$$

$$\rho_g \epsilon_s \left[\frac{\partial}{\partial t} \boldsymbol{v}_s + \boldsymbol{v}_s \cdot \nabla \boldsymbol{v}_s \right] = \sum_p g\, |x - x_p| \int_{S_p} \bar{\bar{\sigma}}_g\, n(y)\, ds_y + \nabla \cdot \bar{\bar{\sigma}}_s + \rho_s \epsilon_s g. \quad (9)$$

The first term on the righthand side of the gas-phase equation of motion represents the effect of stresses in the gas phase, the second term on the righthand side represents the traction exerted on the gas phase by the particle surfaces, and the third term represents the gravity force on the fluid. The first term on the righthand side of the solid-phase equation of motion represents the forces exerted on the particles by the fluid, the second term on the righthand side represents the force due to solid–solid contacts, which can be described using concepts from kinetic theory, and the third term represents the gravity force on the particles. The averaged shear tensor of the gas phase can be rewritten with the Newtonian definition as

$$\bar{\bar{\sigma}}_g = -P_g \bar{\bar{I}} + \frac{\mu_g}{\epsilon_g} \left[\nabla \boldsymbol{v}_g + (\nabla \boldsymbol{v}_g)^T \right], \quad (10)$$

where the gas-phase volume-fraction is introduced in the volume process.

Note that the forces due to fluid traction are treated differently in the fluid-phase and solid-phase momentum balances. In the particle phase, only the resultant force acting on the center of the particle is relevant; the distribution of stress within each particle is not needed to determine its motion. Hence, in the solid-phase momentum balance, the resultant forces due to fluid traction acting everywhere on the surface of the particles are calculated first, after which these are averaged to the particle centers. In the fluid-phase momentum balance, the traction forces at all elements of fluid–solid interaction are calculated, and then are averaged to the location of the surface elements. Hence, the fluid-phase traction term is given as

$$\sum_p \int_{S_p} \bar{\bar{\sigma}}_g \cdot n(y)\, g\, |x - y|\, ds_y = \sum_p g\, |x - x_p| \int_{S_p} \bar{\bar{\sigma}}_g \cdot n(y)\, ds_y - \nabla \cdot \left\{ a \sum_p g\, |x - x_p| \int_{S_p} \left[\bar{\bar{\sigma}}_g \cdot n(y) \right] n(y)\, ds_y \right\} + O(\nabla^2), \quad (11)$$

which is a result of a Taylor series expansion in $g\,|x - y|$ about the center of the particle with radius a. Here terms of $O(\nabla^2)$ and higher have been neglected. Note that the first term on the righthand side of Eq. 11 is the same as the fluid traction term in the particle-phase momentum balance. The difference in the manner in which the resultant forces due to fluid tractions act on the surfaces of the particles is a key distinction between the Jackson (1997) and Ishii (1975) formulations. In the Ishii (1975) formulation, applicable to fluid droplets, the fluid-droplet traction term is the same in the gas phase and the dispersed-phase governing equations.

The integrals involving the traction on a particle surface have been derived by Nadim and Stone (1991) and are given in Jackson (1997) as

$$\sum_p g\, |x - x_p| \int_{S_p} \bar{\bar{\sigma}}_g \cdot n(y)\, ds_y = \frac{\beta}{\epsilon_g} (\boldsymbol{v}_g - \boldsymbol{v}_s) + \rho_g \epsilon_s g + \rho_g \epsilon_s \frac{D_f \boldsymbol{v}_g}{Dt} \quad (12)$$

$$\nabla \cdot \left[a \sum_p g\, |x - x_p| \int_{S_p} \left[\bar{\bar{\sigma}}_g \cdot n(y) \right] n(y)\, ds_y \right] = -\nabla (\epsilon_s P_g), \quad (13)$$

where β is the interphase momentum transfer coefficient. The final equations of motion for both phases according to Jackson (1997) are shown in Table 1, both in the form as

Table 1. Governing Equations Applied to Gas–Solid Flow

Continuity equations

$$\frac{\partial \epsilon_g}{\partial t} + \nabla \cdot (\epsilon_g \boldsymbol{v}_g) = 0$$

$$\frac{\partial \epsilon_s}{\partial t} + \nabla \cdot (\epsilon_s \boldsymbol{v}_s) = 0$$

Momentum equations of Jackson (1997)

$$\rho_g \left[\frac{\partial \boldsymbol{v}_g}{\partial t} + \boldsymbol{v}_g \cdot \nabla \boldsymbol{v}_g \right] = \nabla \cdot \bar{\bar{\tau}}_g - \nabla P - \frac{\beta}{\epsilon_g} (\boldsymbol{v}_g - \boldsymbol{v}_s) + \rho_g g$$

$$\rho_s \epsilon_s \left[\frac{\partial \boldsymbol{v}_s}{\partial t} + \boldsymbol{v}_s \cdot \nabla \boldsymbol{v}_s \right] - \rho_g \epsilon_s \left[\frac{\partial \boldsymbol{v}_g}{\partial t} + \boldsymbol{v}_g \cdot \nabla \boldsymbol{v}_g \right] = \frac{\beta}{\epsilon_g} (\boldsymbol{v}_g - \boldsymbol{v}_s) + \epsilon_s (\rho_s - \rho_g) g + \nabla \cdot \bar{\bar{\tau}}_s - \nabla P_s$$

in alternative form:

$$\rho_g \epsilon_g \left[\frac{\partial \boldsymbol{v}_g}{\partial t} + \boldsymbol{v}_g \cdot \nabla \boldsymbol{v}_g \right] = \epsilon_g \nabla \cdot \bar{\bar{\tau}}_g - \epsilon_g \nabla P - \beta (\boldsymbol{v}_g - \boldsymbol{v}_s) + \epsilon_g \rho_g g$$

$$\rho_s \epsilon_s \left[\frac{\partial \boldsymbol{v}_s}{\partial t} + \boldsymbol{v}_s \cdot \nabla \boldsymbol{v}_s \right] = \epsilon_s \nabla \cdot \bar{\bar{\tau}}_g - \epsilon_s \nabla P + \nabla \cdot \bar{\bar{\tau}}_s - \nabla P_s + \beta (\boldsymbol{v}_g - \boldsymbol{v}_s) + \epsilon_s \rho_s g$$

Momentum equations of Ishii (1975)

$$\rho_g \epsilon_g \left[\frac{\partial \boldsymbol{v}_g}{\partial t} + \boldsymbol{v}_g \cdot \nabla \boldsymbol{v}_g \right] = -\epsilon_g \nabla P + \nabla \cdot \epsilon_g \bar{\bar{\tau}}_g + \epsilon_g \rho_g g - \beta (\boldsymbol{v}_g - \boldsymbol{v}_s)$$

$$\rho_s \epsilon_s \left[\frac{\partial \boldsymbol{v}_s}{\partial t} + \boldsymbol{v}_s \cdot \nabla \boldsymbol{v}_s \right] = -\epsilon_s \nabla P + \nabla \cdot \epsilon_s \bar{\bar{\tau}}_s + \epsilon_s \rho_s g + \beta (\boldsymbol{v}_g - \boldsymbol{v}_s)$$

applied to gas-solid flow (Enwald et al., 1996):

$$\rho_g \epsilon_g \left[\frac{\partial \boldsymbol{v}_g}{\partial t} + \boldsymbol{v}_g \cdot \nabla \boldsymbol{v}_g \right] = -\epsilon_g \nabla P + \nabla \cdot \epsilon_g \bar{\bar{\tau}}_g + \epsilon_g \rho_g g - \beta (\boldsymbol{v}_g - \boldsymbol{v}_s)$$

$$\rho_s \epsilon_s \left[\frac{\partial \boldsymbol{v}_s}{\partial t} + \boldsymbol{v}_s \cdot \nabla \boldsymbol{v}_s \right] = -\epsilon_s \nabla P + \nabla \cdot \bar{\bar{\tau}}_s - \nabla P_s + \epsilon_s \rho_s g + \beta (\boldsymbol{v}_g - \boldsymbol{v}_s)$$

Definitions

$$\bar{\bar{\tau}}_i = 2 \mu_i \bar{\bar{D}}_i + \left(\lambda_i - \frac{2}{3} \mu_i \right) \mathrm{tr}(\bar{\bar{D}}_i) \bar{\bar{I}}$$

$$\bar{\bar{D}}_i = \frac{1}{2} [\nabla \boldsymbol{v}_i + (\nabla \boldsymbol{v}_i)^T]$$

Note: The explanation of the symbols can be found in the Notation.

originally presented in his article, and in an equivalent alternative form, which is merely a linear combination of the original equations.

In Ishii's (1975) formulation, the fluid and dispersed phases are averaged over a fixed volume. This volume is relatively large compared to the size of individual molecules or particles. A phase indicator function is introduced, $X(r)$, which is unity when the point r is occupied by the dispersed phase, and zero if it is not. Averaging over this function leads to the volume fraction of both phases:

$$\epsilon_s = \frac{1}{V}\int_V X(r)\, dV_r, \tag{14}$$

where V is the averaging volume. Since both the continuous and dispersed phases are liquids, they are treated the same in the averaging process. Hence, the momentum balances for both phases are the same,

$$\frac{\partial \epsilon_k \rho_k < \boldsymbol{v}_k >}{\partial t} + \nabla\cdot(\epsilon_k \rho_k < \boldsymbol{v}_k > < \boldsymbol{v}_k >) = -\nabla(\epsilon_k < P_k >) + \nabla\cdot(\epsilon_k < \bar{\bar{\tau}}_k >) + \epsilon_k \rho_k \boldsymbol{g} + \boldsymbol{M}_k, \tag{15}$$

where k is the phase number and $\boldsymbol{M}_k$ is the interphase momentum exchange between the phases, with $\boldsymbol{M}_g + \boldsymbol{M}_s = 0$. In the Ishii (1975) formulation, the distribution of stress within both phases is important since the dispersed phase is considered as fluid droplets. Hence, ''jump'' conditions are used to determine $\boldsymbol{M}_k$. The interphase momentum transfer is defined as

$$\begin{aligned}\boldsymbol{M}_k &= -\sum_j \frac{1}{L_j}(P_k \boldsymbol{n}_k - \boldsymbol{n}_k\cdot\bar{\bar{\tau}}_k) \\ &= \sum_j \frac{1}{L_j}((< P_{ki} > - P_k)\boldsymbol{n}_k - < P_{ki} > \boldsymbol{n}_k - \boldsymbol{n}_k \\ &\qquad \cdot(< \bar{\bar{\tau}}_{ki} > - \bar{\bar{\tau}}_k) + \boldsymbol{n}_k\cdot < \bar{\bar{\tau}}_{ki} >),\end{aligned} \tag{16}$$

where L_j is the interfacial area per unit volume, P_k is the pressure in the bulk of phase k, $< P_{ki} >$ is the average pressure of phase k at the interface, $\bar{\bar{\tau}}_k$ denotes the shear stress in the bulk, and $< \bar{\bar{\tau}}_{ki} >$ represents the average shear stress at the interface. The terms $(< P_{ki} > - P_k)\boldsymbol{n}_k$ and $\boldsymbol{n}_k\cdot(< \bar{\bar{\tau}}_{ki} > - \bar{\bar{\tau}}_k)$ are identified by Ishii (1975) as the form drag and the skin drag, respectively, making up the total drag force. The other terms can be written out as

$$\boldsymbol{M}_k = \text{drag} + < P_k > \nabla\epsilon_k + (< P_{ki} > - < P_k >)\nabla\epsilon_k - (\nabla\epsilon_k)\cdot < \bar{\bar{\tau}}_{ki} >. \tag{17}$$

According to Ishii and Mishima (1984), the last term on the righthand side is an interfacial shear term and is important in a separated flow. According to Ishii (1975), the term $(< P_{ki} > - < P_k >)$ only plays a role when the pressure at the bulk is significantly different from that at the interface, as in stratified flows. For many applications both terms are negligible, and

$$\boldsymbol{M}_k = \text{drag} + < P_k > \nabla\epsilon_k. \tag{18}$$

The momentum equations for the gas phase and the dispersed phase following the original work of Ishii (1975) are shown in Table 1. Many researchers and commercial codes modify Ishii's (1975) equations to describe gas–solid flows (such as Enwald et al., 1996). These modified equations are also shown in Table 1. When Ishii's (1975) equations are applied to gas–solid flows, the solid-phase stress tensor is not multiplied by the solid volume fraction, since the volume-fraction functionality is already accounted for in the kinetic theory description.

Comparing the Ishii (1975) and Jackson (1997) momentum balances, the differences are twofold. First, Jackson (1997) includes the solid volume fraction multiplied by the gradient of the total gas-phase stress tensor in the solid-phase momentum balance, whereas Ishii (1975) only includes the solid volume-fraction multiplied by the gradient of the pressure. Second, in the Ishii (1975) approach in the gas-phase momentum balance, the pressure carries the gas volume fraction outside the gradient operator; the shear stress carries the gas volume fraction inside the gradient operator. In Jackson (1997) both stresses are treated equally with respect to the gas volume fraction and the gradient operators. When the gas-phase shear stress plays an important role, these differences may be significant near large gradients of volume fraction, that is, near bubbles or surfaces.

Closure Relations

Kinetic theory

Closure of the solid-phase momentum equation requires a description for the solid-phase stress. When the particle motion is dominated by collisional interactions, concepts from gas kinetic theory (Chapman and Cowling, 1970) can be used to describe the effective stresses in the solid phase resulting from particle streaming (kinetic contribution) and direct collisions (collisional contribution). Constitutive relations for the solid-phase stress based on kinetic theory concepts have been derived by Lun et al. (1984), allowing for the inelastic nature of particle collisions.

Analogous to the thermodynamic temperature for gases, the granular temperature can be introduced as a measure of the particle velocity fluctuations.

$$\Theta = \frac{1}{3} < \boldsymbol{v}_s'^2 >. \tag{19}$$

Since the solid-phase stress depends on the magnitude of these particle-velocity fluctuations, a balance of the granular energy ($\frac{3}{2}\Theta$) associated with these particle-velocity fluctuations is required to supplement the continuity and momentum balance for both phases. This balance is given as

$$\frac{3}{2}\left[\frac{\partial}{\partial t}(\epsilon_s\ \rho_s\Theta) + \nabla\cdot(\epsilon_s \rho_s \Theta \boldsymbol{v}_s)\right] = \left(-\nabla P_s \bar{\bar{I}} + \bar{\bar{\tau}}_s\right):\nabla \boldsymbol{v}_s - \nabla\cdot(\kappa_s\nabla\Theta) - \gamma_s - J_s, \tag{20}$$

where the first term on the righthand side represents the creation of fluctuating energy due to shear in the particle phase, the second term represents the diffusion of fluctuating energy along gradients in Θ, γ_s represents the dissipation due to inelastic particle–particle collisions, and J_s represents the dissipation or creation of granular energy resulting from the working of the fluctuating force exerted by the gas through the fluctuating velocity of the particles. Rather than solving the complete granular energy balance given in Eq. 20, some researchers (Syamlal et al., 1993; Boemer et al., 1995; Van Wachem et al., 1998, 1999) assume the granular energy is in a steady state and dissipated locally, and neglect convection and diffusion. Retaining only the generation and the dissipation terms, Eq. 20 simplifies to an algebraic expression for the granular temperature:

$$0 = \left(-\nabla P_s \bar{\bar{I}} + \bar{\bar{\tau}}_s\right) : \nabla \boldsymbol{v}_s - \gamma_s. \tag{21}$$

Because the generation and dissipation terms dominate in dense-phase flows, it is anticipated that this simplification is a reasonable one in dense regions of flow.

Solid-phase stress tensor

The solids pressure represents the normal solid-phase forces due to particle–particle interactions. In the literature there is general agreement on the form of the solids pressure, given by Lun et al. (1984) as

$$\begin{aligned} P_s &= \rho_s \epsilon_s \Theta \left[1 + 2(1+e) g_0 \epsilon_s\right] \\ &= \rho_s \epsilon_s \Theta + 2 g_0 \rho_s \epsilon_s^2 \Theta (1+e). \end{aligned} \tag{22}$$

The first part of the solids pressure represents the kinetic contribution, and the second part represents the collisional contribution. The kinetic part of the stress tensor physically represents the momentum transferred through the system by particles moving across imaginary shear layers in the flow; the collisional part of the stress tensor denotes the momentum transferred by direct collisions.

The solids bulk viscosity describes the resistance of the particle suspension against compression. In the literature, there also is general agreement on the form of the solids bulk viscosity, given by Lun et al. (1984) as

$$\lambda_s = \frac{4}{3} \epsilon_s^2 \rho_s d_s g_0 (1+e) \sqrt{\frac{\Theta}{\pi}}. \tag{23}$$

However, the kinetic theory description for the solids shear viscosity often differs between the various two-fluid models. Gidaspow (1994) does not account for the inelastic nature of particles in the kinetic contribution of the total stress, as Lun et al. (1984) do, claiming this correction is negligible. The solids shear viscosity of Syamlal et al. (1993) neglects the kinetic or streaming contribution, which dominates in dilute-phase flow. Hrenya and Sinclair (1997) follow Lun et al. (1984), but constrain the mean free path of the particle by a dimension characteristic of the actual physical system. This is opposed to the Lun et al. (1984) theory, which allows the mean free path to tend toward infinity, and the solids viscosities tends toward a finite value as the solid volume fraction tends to zero. Hence, by constraining the mean free path, the limit of the Hrenya and Sinclair (1997) shear viscosity expression correctly tends to zero as the solid volume fraction approaches zero. In dense solid systems ($\epsilon_s > 0.05$), there is no difference in the predicted solids viscosity of Lun et al. (1984) and Hrenya and Sinclair (1997). The Syamlal et al. (1993) solids shear viscosity also tends to zero as the solid volume fraction tends to zero. In this case, however, this solids shear

Table 2. Solids Shear Viscosity

Lun et al. (1984)

$$\begin{aligned} \mu_s &= \frac{5\sqrt{\tau\Theta}}{96} \rho_s d_s \left[\left(\frac{1}{\eta g_0} + \frac{8\epsilon_s}{5} \right) \left(\frac{1 + \frac{8}{5}\eta(3\eta - 2)\epsilon_s g_0}{2 - \eta} \right) + \frac{768}{25\pi} \eta \epsilon_s^2 g_0 \right] \\ &= \frac{4}{5} \epsilon_s^2 \rho_s d_s g_0 (1+e) \sqrt{\frac{\Theta}{\pi}} + \frac{1}{15} \sqrt{\Theta\pi} \frac{\rho_s d_s g_0 (1+e)(3/2\, e - 1/2)\epsilon_s^2}{(3/2 - 1/2\, e)} \\ &\quad + \frac{1}{6} \sqrt{\Theta\pi} \frac{\rho_s d_s \epsilon_s (3/4\, e + 1/4)}{(3/2 - e/2)} + \frac{10}{96} \sqrt{\Theta\pi} \frac{\rho_s d_s}{(1+e)(3/2 - 1/2\, e) g_0} \end{aligned}$$

Syamlal et al. (1993)

$$\begin{aligned} \mu_s &= \frac{4}{5} \epsilon_s^2 \rho_s d_s g_0 (1+e) \sqrt{\frac{\Theta}{\pi}} + \frac{\epsilon_s d_s \rho_s \sqrt{\pi\Theta}}{6(3-e)} \left[1 + \frac{2}{5}(1+e)(3e-1)\epsilon_s g_0 \right] \\ &= \frac{4}{5} \epsilon_s^2 \rho_s d_s g_0 (1+e) \sqrt{\frac{\Theta}{\pi}} + \frac{1}{15} \sqrt{\Theta\pi}\, \rho_s d_s g_0 \frac{(1+e)(3/2\, e - 1/2)}{(3/2 - e/2)} \epsilon_s^2 \\ &\quad + \frac{1}{12} \frac{\epsilon_s d_s \rho_s \sqrt{\pi\Theta}}{(3/2 - e/2)} \end{aligned}$$

Gidaspow (1994)

$$\begin{aligned} \mu_s &= \frac{4}{5} \epsilon_s^2 \rho_s d_s g_0 (1+e) \sqrt{\frac{\Theta}{\pi}} + \frac{2\frac{5\sqrt{\pi}}{96} \rho_s d_s \sqrt{\Theta}}{(1+e) g_0} \cdot \left[1 + \frac{4}{5} g_0 \epsilon_s (1+e) \right]^2 \\ &= \frac{4}{5} \epsilon_s^2 \rho_s d_s g_0 (1+e) \sqrt{\frac{\Theta}{\pi}} + \frac{1}{15} \sqrt{\Theta\pi}\, \rho_s d_s g_0 (1+e) \epsilon_s^2 \\ &\quad + \frac{1}{6} \sqrt{\Theta\pi}\, \rho_s d_s \epsilon_s + \frac{10}{96} \sqrt{\Theta\pi} \frac{\rho_s d_s}{(1+e) g_0} \end{aligned}$$

Hrenya and Sinclair (1997)

$$\begin{aligned} \mu_s &= \frac{5\sqrt{\pi\Theta}}{96} \rho_s d_s \left[\left(\frac{1}{1 + \frac{\lambda_{mfp}}{R}} \frac{1}{\eta g_0} + \frac{8\epsilon_s}{5} \right) \left(\frac{1 + 8/5\,\eta(3\eta - 2)\epsilon_s g_0}{2 - \eta} \right) + \frac{768}{25\pi} \eta \epsilon_s^2 g_0 \right] \\ &= \frac{4}{5} \epsilon_s^2 \rho_s g_0 (1+e) \sqrt{\frac{\Theta}{\pi}} + \frac{1}{15} \sqrt{\Theta\pi} \frac{\rho_s d_s g_0 (1+e)(3/2\, e - 1/2)\epsilon_s^2}{(3/2 - e/2)} \\ &\quad + \frac{1}{6} \sqrt{\Theta\pi} \frac{\rho_s d_s \epsilon_s \left(1/2 \left(1 + \frac{\lambda_{mfp}}{R} \right) + 3/4\, e - 1/4 \right)}{(3/2 - 1/2\, e) \left(1 + \frac{\lambda_{mfp}}{R} \right)} \\ &\quad + \frac{10}{96} \sqrt{\Theta\pi} \frac{\rho_s d_s}{(1+e)(3/2 - 1/2\, e) g_0 \left(1 + \frac{\lambda_{mfp}}{R} \right)} \end{aligned}$$

Note: The symbols can be found in the Notation.

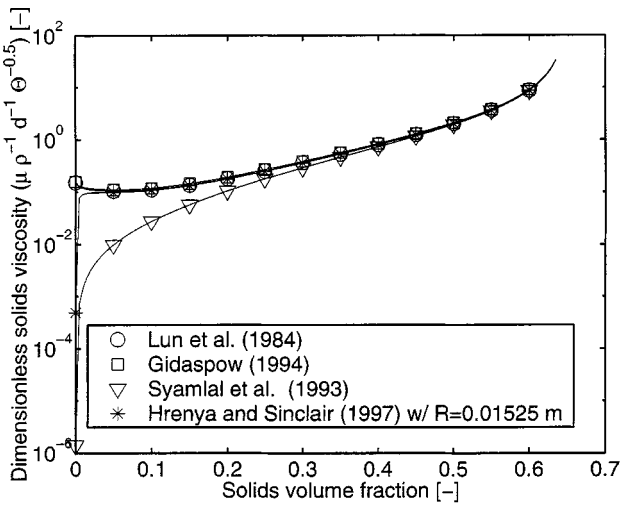

Figure 1. Comparison of solids shear viscosities from different kinetic theory models: $e = 0.9$, $\epsilon_{max} = 0.65$.

viscosity limit is reached because the kinetic contribution to the solids viscosity is neglected.

Table 2 presents the forms for the solids shear viscosity as presented in the original articles as well as in an equivalent form so that all of the models can be easily compared. Figure 1 shows a comparison of the constitutive models for the solids shear viscosity as a function of the solid volume fraction. All models yield the same solids shear viscosity at high solids volume fractions. Syamlal et al. (1993) deviate from the others for solid volume fractions less than 0.3. Hrenya and Sinclair (1997) show a rapid decrease in solids shear viscosity at extremely small particle concentrations.

Conductivity of granular energy

Similar to the solids shear viscosity, the solids thermal conductivity, κ, consists of a kinetic contribution and a collisional contribution. Gidaspow (1994) differs from Lun et al. (1984) only in the dependency of the solids thermal conductivity on the coefficient of restitution. Syamlal et al. (1993) neglect the kinetic contribution to the thermal conductivity. Hrenya and Sinclair (1997) follow Lun et al. (1984), but constrain the mean free path of the particle by a dimension characteristic of the actual system. Hence, the limit of their conductivity expression, as with the shear viscosity, correctly tends to zero when approaching zero solid volume fraction. Syamlal et al. (1993) also correctly predict zero for the conductivity at zero solid volume fraction by neglecting the kinetic contribution.

Table 3 presents the forms for the solids thermal conductivity as presented in the original articles, as well as in an equivalent form so that all of the closure models can be easily compared. Figure 2 shows a quantitative comparison of the constitutive models for the solids thermal conductivity as a function of the solid volume fraction. All models yield the same thermal conductivity at high solid volume fraction. Syamlal et al. (1993) deviate from the others for solids volume fraction less than 0.3. Hrenya and Sinclair (1997) show a

Table 3. Solids Thermal Conductivities

Lun et al. (1984)

$$\kappa = \frac{25\sqrt{\pi\Theta}}{128}\rho_s d_s\left[\left(\frac{8}{\eta g_0}+\frac{96\epsilon_s}{5}\right)\left(\frac{1+12/5\eta^2(4\eta-3)\epsilon_s g_0}{41-33\eta}\right)+\frac{512}{25\pi}\eta\epsilon_s^2 g_0\right]$$

$$= 2\epsilon_s^2\rho_s d_s g_0(1+e)\sqrt{\frac{\Theta}{\pi}}+\frac{9}{8}\sqrt{\Theta\pi}\frac{\rho_s d_s g_0(1/2+\epsilon/2)^2(2e-1)\epsilon_s^2}{(49/16-33/16e)}+\frac{15}{16}\sqrt{\Theta\pi}\frac{\epsilon_s\rho_s d_s(e^2/2+1/4e+1/4)}{(49/16-33/16e)}+\frac{25}{64}\sqrt{\Theta\pi}\frac{\rho_s d_s}{(1+e)(49/16-33/16e)g_0}$$

Syamlal et al. (1993)

$$\kappa = \frac{15 d_s\rho_s\epsilon_s\sqrt{\Theta\pi}}{4(41-33\eta)}\left[1+\frac{12}{5}\eta^2(4\eta-3)\epsilon_s g_0+\frac{16}{15\pi}(41-33\eta)\eta\epsilon_s g_0\right]$$

$$= 2\epsilon_s^2\rho_s d_s g_0(1+e)\sqrt{\frac{\Theta}{\pi}}+\frac{9}{8}\sqrt{\Theta\pi}\frac{\rho_s d_s g_0(1/2+e/2)^2(2e-1)\epsilon_s^2}{(49/16-33/16e)}+\frac{15}{32}\sqrt{\Theta\pi}\frac{\epsilon_s\rho_s d_s}{(49/16-33/16e)}$$

Gidaspow (1994)

$$\kappa_{dil} = \frac{75}{384}\rho_s d_s\sqrt{\pi\Theta}$$

$$\kappa = \frac{2}{(1+e)g_0}\left[1+\frac{6}{5}(1+e)g_0\epsilon_s\right]^2\kappa_{dil}+2\epsilon_s^2\rho_s d_s g_0(1+e)\sqrt{\frac{\Theta}{\pi}}$$

$$= 2\epsilon_s^2\rho_s d_s g_0(1+e)\sqrt{\frac{\Theta}{\pi}}+\frac{9}{8}\sqrt{\Theta\pi}\frac{\rho_s d_s g_0(1/2+e/2)^2(2e-1)\epsilon_s^2}{(49/16-33/16e)}+\frac{15}{16}\sqrt{\Theta\pi}\frac{\epsilon_s\rho_s d_s\left(e^2/2+1/4e+1/4+\frac{\lambda_{mfp}}{R}\right)}{(49/16-33/16e)\left(1+\frac{\lambda_{mfp}}{R}\right)}+\frac{25}{64}\sqrt{\Theta\pi}\frac{\rho_s d_s}{(1+e)(49/16-33/16e)\left(1+\frac{\lambda_{mfp}}{R}\right)g_0}$$

Note: The symbols can be found in the Notation.

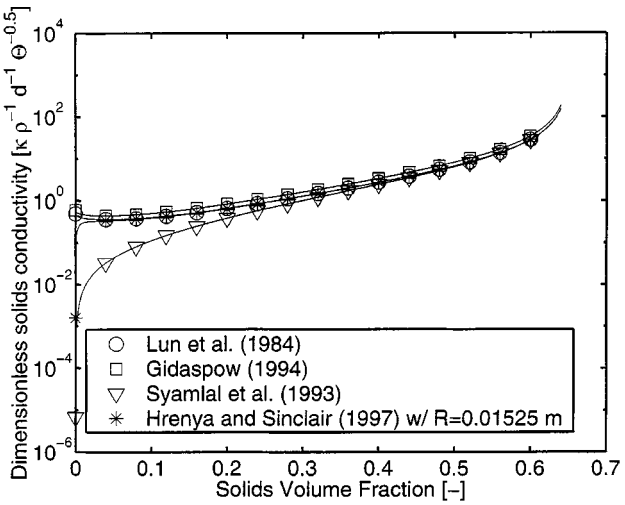

Figure 2. Comparison of solids thermal conductivity from different kinetic theory models: $e = 0.9$, $\epsilon_{max} = 0.65$.

rapid decrease in thermal conductivity at extremely small particle concentration.

Dissipation and generation of granular energy

Jenkins and Savage (1983) represent the dissipation of granular energy due to inelastic particle–particle collisions as

$$\gamma_s = 3(1-e^2)\epsilon_s^2\rho_s g_0\Theta\left(\frac{4}{d_s}\sqrt{\frac{\Theta}{\pi}} - \nabla\cdot\boldsymbol{v}_s\right). \qquad (24)$$

For small mean-field gradients associated with a slight particle inelasticity, the term $\nabla\cdot\boldsymbol{v}_s$ is typically omitted, as in Lun et al. (1984):

$$\gamma_s = 12(1-e^2)\frac{\epsilon_s^2\rho_s g_0}{d_s\sqrt{\pi}}\Theta^{3/2}. \qquad (25)$$

The rate of energy dissipation per unit volume resulting from the action of the fluctuating force exerted by the gas through the fluctuating velocity of the particles is given by $J_s = \beta(\overline{\boldsymbol{v}_s'\cdot\boldsymbol{v}_s'} - \overline{\boldsymbol{v}_g'\cdot\boldsymbol{v}_s'})$. According to Gidaspow (1994), the term $\overline{\boldsymbol{v}_s'\cdot\boldsymbol{v}_s'}$ is equal to 3Θ. The second term, $\overline{\boldsymbol{v}_g'\cdot\boldsymbol{v}_s'}$, is neglected by Gidaspow (1994). However, Louge et al. (1991) have proposed a closure for this second term based on the work of Koch (1990) for the dilute flow regime, which we apply here:

$$J_s = \beta\left[3\Theta - \frac{\beta d_s(\boldsymbol{v}_g-\boldsymbol{v}_s)^2}{4\epsilon_s\rho_s\sqrt{\pi\Theta}}\right]. \qquad (26)$$

Using the closure of Louge et al. (1991) for $\overline{\boldsymbol{v}_g'\cdot\boldsymbol{v}_s'}$, we have found that this term is of the same order of magnitude as $\overline{\boldsymbol{v}_s'\cdot\boldsymbol{v}_s'}$. It should be noted, however, that the term as proposed by Louge et al. (1991) is originally meant for the dilute flow regime and does not tend to zero at closest solids packing. Therefore, Sundaresan (private communication, 1999) has proposed dividing this term by the radial distribution function to correct the closure in this limit of closest solids packing.

Recently, Sangani et al. (1996) have derived an equation for $\overline{\boldsymbol{v}_s'\cdot\boldsymbol{v}_s'}$, and Koch and Sangani (1999) have derived an equation for $\overline{\boldsymbol{v}_g'\cdot\boldsymbol{v}_s'}$, especially for dense solid flows. With these correlations, the expression for the rate of energy dissipation resulting from fluctuations is

$$J_s = \left[3\frac{\mu_s\epsilon_s\Theta}{d_s^2}R_{\text{diss}} - \frac{\beta^2 d_s(\boldsymbol{v}_g-\boldsymbol{v}_s)^2}{4\epsilon_s\rho_s\sqrt{\pi\Theta}}S^*\right], \qquad (27)$$

where R_{diss} can be interpreted as the effective drag coefficient, which is determined as a result of a fit of numerical simulations (Sangani et al., 1996), and S^* is an energy source:

$$S^* = \frac{1}{2\sqrt{\pi}}R_s\beta^2, \qquad (28)$$

where R_s represents the energy source due to a specified mean force acting on the particles and is obtained by a fit of numerical simulations. When the solids volume fraction approaches the maximum packing limit, R_s tends to zero.

Table 4. Radial Distribution Function

Carnahan and Starling (1969) $$g_0 = \frac{1}{1-\epsilon_s} + \frac{3\epsilon_s}{2(1-\epsilon_s)^2} + \frac{\epsilon_s^2}{2(1-\epsilon_s)^3}$$
Lun and Savage (1986) $$g_0 = \left(1-\frac{\epsilon_s}{\epsilon_{s,\max}}\right)^{-2.5\epsilon_{s,\max}}$$
Sinclair and Jackson (1989) $$g_0 = \left[1-\left(\frac{\epsilon_s}{\epsilon_{s,\max}}\right)^{1/3}\right]^{-1}$$
Gidaspow (1994) $$g_0 = \frac{3}{5}\left[1-\left(\frac{\epsilon_s}{\epsilon_{s,\max}}\right)^{1/3}\right]^{-1}$$

Radial distribution function

The solid-phase stress is dependent on the radial distribution function at contact. Lun et al. (1984) employed the Carnahan and Starling (1969) expression for the radial distribution function. The Carnahan and Starling (1969) expression, however, does not tend toward the correct limit at closest solids packing. Because particles are in constant contact at the maximum solid volume fraction, the radial distribution function at contact tends to infinity. Therefore, alternative expressions to the Carnahan and Starling (1969) expression have been proposed by Gidaspow (1994), Lun and Savage (1986), and Sinclair and Jackson (1989), which tend to the correct limit at closest packing. These various forms of the radial distribution function are given in Table 4 and are plotted in Figure 3 as a function of the solid volume fraction, along with the data from molecular simulations of Alder and Wainright (1960) and the data from experiments of Gidaspow and Huilin (1998). The expression of Gidaspow (1994) most closely coincides with the data over the widest range of solid volume fractions. The expression of Gidaspow (1994), how-

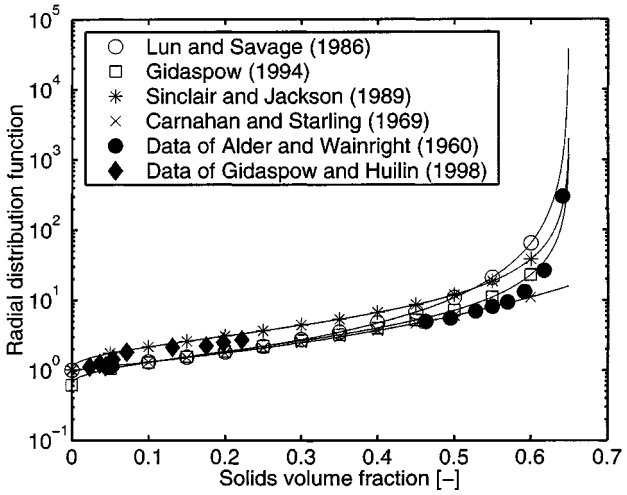

Figure 3. Radial distribution functions: computational data of Alder and Wainright (1960) vs. experimental data of Gidaspow and Huilin (1998).

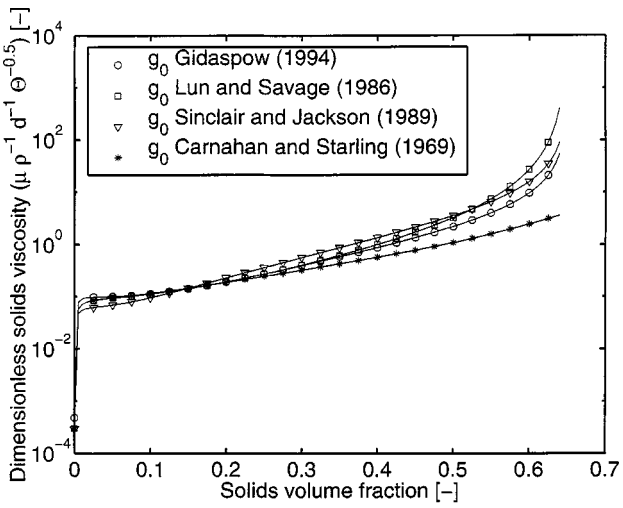

Figure 4. Solids shear viscosity from different radial distribution functions.

Solids shear viscosity follows Hrenya and Sinclair (1997); $e = 0.9$, $R = 0.01525$ m, and $\epsilon_{max} = 0.65$.

ever, does not approach the correct limit of one as the solid volume-fraction approaches zero. Figure 4 presents the effect of these different expressions for the radial distribution functions on the solids shear viscosity. A difference of up to a factor of 2 in viscosity can result.

Frictional stress

At high solid volume fraction, sustained contacts between particles occur. The resulting frictional stresses must be accounted for in the description of the solid-phase stress. Zhang and Rauenzahn (1997) conclude that particle collisions are no longer instantaneous at very high solid volume fractions, as is assumed in kinetic theory. Several approaches most of which originated from geological research groups, have been presented in the literature to model the frictional stress. The models for frictional stress are very empirical and should be used with caution. Typically, the frictional stress, $\bar{\bar{\sigma}}_f$, is written in a Newtonian form:

$$\bar{\bar{\sigma}}_f = P_f \bar{\bar{I}} + \mu_f \left[\nabla \boldsymbol{v} + (\nabla \boldsymbol{v})^T \right]. \tag{29}$$

The frictional stress is added to the stress predicted by kinetic theory for $\epsilon_s > \epsilon_{s,\min}$:

$$P_s = P_{\text{kinetic}} + P_f \tag{30}$$

$$\mu_s = \mu_{\text{kinetic}} + \mu_f. \tag{31}$$

Johnson and Jackson (1987) propose a semiempirical equation for the normal frictional stress, P_f:

$$P_f = Fr \frac{(\epsilon_s - \epsilon_{s,\min})^n}{(\epsilon_{s,\max} - \epsilon_s)^p}, \tag{32}$$

where Fr, n, and p are empirical material constants, and $\epsilon_s > \epsilon_{s,\min}$, $\epsilon_{s,\min}$ are the solid-volume fraction when frictional stresses become important; Fr, n, and p are material-dependent constants. The frictional shear viscosity is then related to the frictional normal stress by the linear law proposed by Coulomb (1776)

$$\sigma_{xy} = P_f \sin \phi, \tag{33}$$

where ϕ is the angle of internal friction of the particle. Representative values for the empirical constants employed in Eqs. 32 and 33 are given in Table 5.

Another approach, originally from Schaeffer (1987), was employed by Syamlal et al. (1993) to describe the frictional stress in very dense gas–solid systems:

$$P_f = A(\epsilon_s - \epsilon_{s,\min})^n \tag{34}$$

$$\mu_f = \frac{P_f \cdot \sin \phi}{\epsilon_s \sqrt{\frac{1}{6}\left[\left(\frac{\partial u_s}{\partial x} - \frac{\partial v_s}{\partial y}\right)^2 + \left(\frac{\partial v_s}{\partial y}\right)^2 + \left(\frac{\partial u_s}{\partial x}\right)^2\right] + \frac{1}{4}\left(\frac{\partial u_s}{\partial y} + \frac{\partial v_s}{\partial x}\right)^2}}. \tag{35}$$

Values of $A = 10^{25}$, $n = 10$, $\epsilon_{s,\min} = 0.59$, and $\phi = 25°$ are typically employed.

The approaches of Johnson and Jackson (1987) and Syamlal et al. (1993) are compared in Figure 5. It can be seen that resulting normal frictional stress can differ by orders of magnitude.

Interphase transfer coefficient

Generally, the form drag and skin drag are combined in one empirical parameter, the interphase drag constant β, in the modeling of the momentum transfer between the two phases. The drag coefficient β is typically obtained experimentally from pressure drop measurements in fixed, fluidized, or settling beds. Ergun (1952) performed measurements in fixed liquid–solid beds at packed conditions to determine the pressure drop. Wen and Yu (1966) have performed settling experiments of solid particles in a liquid over a wide range of solid volume fractions, and have correlated

Table 5. Empirical Parameters of Eqs. 32 and 33 by Various Researchers

Fr [N/m^2]	n	p	$\epsilon_{s_{min}}$	ϕ	d_s [μm]	ρ_s [kg/m^3]	Material	Reference
0.05	2	3	0.5	28°	150	2500	Not specified	Ocone et al. (1993)
3.65×10^{-32}	0	40	—	25.0°	1800	2980	Glass	Johnson and Jackson (1987)
4.0×10^{-32}	0	40	—	25.0°	1000	1095	Polystyrene	Johnson and Jackson (1987)
0.05	2	5	0.5	28.5°	1000	2900	Glass	Johnson et al. (1990)

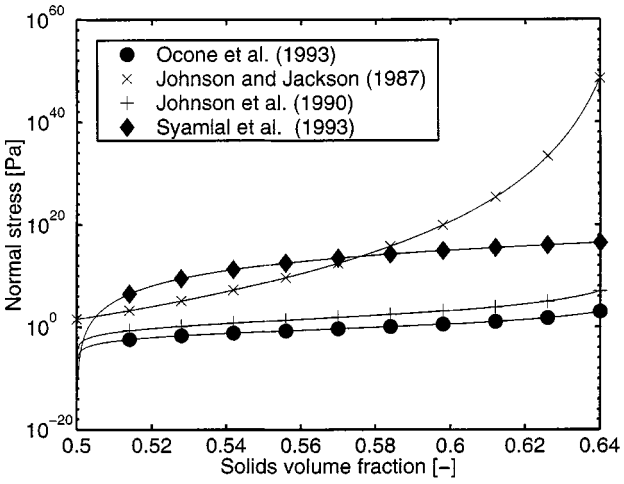

Figure 5. Different expressions for the frictional normal stress.

their data and those of others for solids concentrations, $0.01 \leq \epsilon_s \leq 0.63$. Syamlal et al. (1993) use the empirical correlations of Richardson and Zaki (1954) and Garside and Al-Bibouni (1977) to determine the terminal velocity in fluidized and settling beds expressed as a function of the solid volume fraction and the particle Reynolds number. From the terminal velocity, the drag force can be readily computed.

The drag model of Gidaspow (1994) follows Wen and Yu (1966) for solid volume fractions lower than 0.2 and Ergun (1952) for solid volume fractions larger than 0.2. The motivation for this hybrid drag description of Gidaspow (1994) is unclear because the Wen and Yu (1966) expression includes experimental drag data for solid volume fractions larger than 0.2. Moreover, a step change in the interphase drag constant is obtained at the ''crossover'' solid volume fraction of 0.2, which can possibly lead to difficulties in numerical convergence. The magnitude of this discontinuity in β increases with increasing particle Reynolds number. The drag coefficients are summarized in Table 6 and are compared quantitatively in Figure 6 for a range of solid volume fractions at a fixed particle Reynolds number.

Simulations

The impact on the predicted flow patterns of the differences in the governing equations and constitutive models are compared for the test cases of a freely bubbling fluidized-bed, a slugging fluidized bed, and a single bubble injection into a fluidized bed. The particles in a fluidized bed move according to the action of the fluid through the drag force, and bubbles and complex solid mixing patterns result. Typically, the average solid volume fraction in the bed is fairly large, averaging about 40%, whereas in the the freeboard of the fluidized bed (the top) there are almost no particles ($\epsilon_s \approx 10^{-6}$).

The simulations in this work were carried out with the commercial CFD code CFX 4.2 from AEA Technology, Harwell, UK, employing the Rhie-Chow (Rhie and Chow, 1983) algorithm for discretization. For solving the difference equa-

Table 6. Drag Coefficients

Wen and Yu (1966)

$$\beta = \frac{3}{4} C_D \frac{(1-\epsilon_s)\epsilon_s \rho_g |\boldsymbol{v}_g - \boldsymbol{v}_s|}{d_s} (1-\epsilon_s)^{-2.65}$$

Rowe (1961)

$$C_D = \begin{cases} \dfrac{24}{Re_p(1-\epsilon_s)}\left[1 + 0.15((1-\epsilon_s)Re_p)^{0.687}\right] & \text{if } (1-\epsilon_s)Re_p < 1{,}000 \\ 0.44 \qquad Re_p = \dfrac{d_s \rho_g |\boldsymbol{v}_g - \boldsymbol{v}_s|}{\mu_g} & \text{if } (1-\epsilon_s)Re_p \geq 1{,}000 \end{cases}$$

Gidaspow (1994) applies the Ergun (1952) equation for higher volume fractions:

$$\beta = \begin{cases} 150\dfrac{\epsilon_s^2 \mu_g}{(1-\epsilon_s)d_s^2} + \dfrac{7}{4}\dfrac{\epsilon_s \rho_g |\boldsymbol{v}_g - \boldsymbol{v}_s|}{d_s} & \text{if } \epsilon_g > 0.2 \\ \dfrac{3}{4} C_D \dfrac{(1-\epsilon_s)\epsilon_s \rho_g |\boldsymbol{v}_g - \boldsymbol{v}_s|}{d_s}(1-\epsilon_s)^{-2.65} & \text{if } \epsilon_s \leq 0.2 \end{cases}$$

Syamlal et al. (1993)

$$\beta = \frac{3}{4} C_D \frac{\epsilon_s(1-\epsilon_s)\rho_g}{V_r^2 d_s} |\boldsymbol{v}_g - \boldsymbol{v}_s|$$

Dalla Valle (1948)

$$C_D = \left(0.63 + 4.8\sqrt{\frac{V_r}{Re}}\right)^2$$

Garside and Al-Dibouni (1977)

$$V_r = \frac{1}{2}\left[a - 0.06\ Re + \sqrt{(0.06Re)^2 + 0.12Re(2b-a) + a^2}\right]$$

$$a = (1-\epsilon_s)^{4.14}$$

$$b = \begin{cases} 0.8(1-\epsilon_s)^{1.28} & \text{if } \epsilon_s \geq 0.15 \\ (1-\epsilon_s)^{2.65} & \text{if } \epsilon_s < 0.15 \end{cases}$$

tions, the higher-order total variation diminishing (TVD) scheme, Superbee is used. This TVD scheme incorporates a modification to the higher-order upwind scheme (second order). The time discretization is done with the second-order backward-difference scheme. The solution of the pressure from the momentum equations requires a pressure correction equation, correcting the pressure and the velocities after each iteration; for this, the SIMPLE (Patankar, 1980) algorithm is employed. The calculated pressure is used to determine the density of the fluid phase; the simulations are performed allowing for compressibility of the gas phase. The grid spacing was determined by refining the grid until average properties changed by less than 4%. Due to the deterministic chaotic nature of the system, the dynamic behavior always changes with the grid. The simulations of the slugging fluidized bed and the freely bubbling fluidized bed were carried out for 25 s of real time. After about 5 s of real time, the simulation has reached a state in which averaged properties stay unchanged. Averaged properties, such as bubble size and bed expansion, were determined by averaging over the last 15 s of real time in each simulation. A bubble is defined as a void in the solid phase with a solid volume fraction less than 15%. The bubble diameter is defined as the diameter of a circle having the same surface as the void in the solid phase; this is called the equivalent bubble diameter.

Boundary conditions

All the simulations are carried out in a two-dimensional rectangular space in which front and back wall effects are neglected. The left and right walls of the fluidized bed are treated as no-slip velocity boundary conditions for the fluid phase, and the free-slip velocity boundary conditions are employed for the particle phase. A possible boundary condition for the granular temperature follows Johnson and Jackson (1987):

$$n\cdot(\kappa\nabla\Theta) = \frac{\pi\rho_s\epsilon_s\sqrt{3\Theta}}{6\epsilon_{s,\max}\left[1-\left(\frac{\epsilon_s}{\epsilon_{s,\max}}\right)^{1/3}\right]}\left[\varphi'\,|\,\boldsymbol{v}_{\text{slip}}\,|^2-\frac{3\Theta}{2}\left(1-e_w^2\right)\right], \quad (36)$$

where the lefthand side represents the conduction of granular energy to the wall, the first term on the righthand side represents the generation of granular energy due to particle slip at the wall, and the second term on the righthand side represents dissipation of granular energy due to inelastic collisions. Another possibility for the boundary condition for the granular temperature is proposed by Jenkins (1992):

$$n\cdot(\kappa\nabla\Theta) = -\boldsymbol{v}_{\text{slip}}\cdot M - D, \quad (37)$$

where the exact formulations of M and D depend upon the amount of friction and sliding occurring at the wall region. Simulations we have done with an adiabatic boundary condition at the wall ($\nabla\Theta = 0$) show very similar results.

The boundary condition at the top of the freeboard (fluid-phase outlet) is a so-called pressure boundary. The pressure at this boundary is fixed to a reference value, 1.013×10^5 Pa. Neumann boundary conditions are applied to the gas flow, requiring a fully developed gas flow. For this, the freeboard of the fluidized bed needs to be of sufficient height; this is validated through the simulations. In the freeboard, the solid volume fraction is very close to zero, and this can lead to unrealistic values for the particle-velocity field and poor convergence. For this reason, a solid volume fraction of 10^{-6} is set at the top of the freeboard. This way the whole freeboard is filled with a very small number of particles, which gives more realistic results for the particle phase velocity in the freeboard, but does not influence the behavior of the fluidized bed itself.

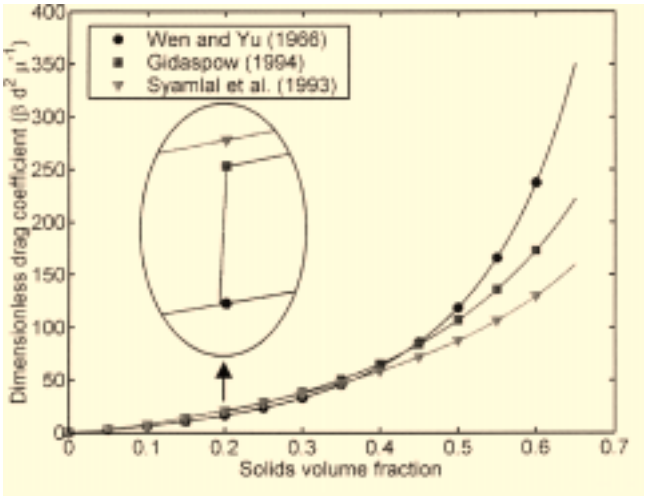

Figure 6. Different expressions for the interphase drag coefficient as a function of solid volume-fraction: $Re_p = 45$.

The bottom of the fluidized bed is made impenetrable for the solid phase by setting the solid phase axial velocity to zero. For the freely bubbling fluidized bed and the slugging fluidized bed, Dirichlet boundary conditions are employed at the bottom with a uniform gas inlet velocity. To break the symmetry in the case of the bubbling and slugging beds, initially a small jet of gas is specified at the bottom lefthand side of the geometry. In the case of the bubble injection, a Dirichlet boundary condition is employed at the bottom of the fluidized bed. The gas inlet velocity is kept at the minimum fluidization velocity, except for a small orifice in the center of the bed, at which a very large inlet velocity is specified. Finally, the solid-phase stress, as well as the granular temperature at the top of the fluidized bed, are set to zero.

Initial conditions

Initially, the bottom part of the fluidized bed is filled with particles at rest with a uniform solid volume fraction. The gas flow in the bed is set to its minimum fluidization velocity. In the freeboard a solid volume fraction of 10^{-6} is set, as explained earlier. The granular temperature is initially set to 10^{-10} $\text{m}^2\cdot\text{s}^{-2}$.

Test Case

With increasing gas velocity above the minimum fluidization velocity, U_{mf}, bubbles are formed as a result of the in-

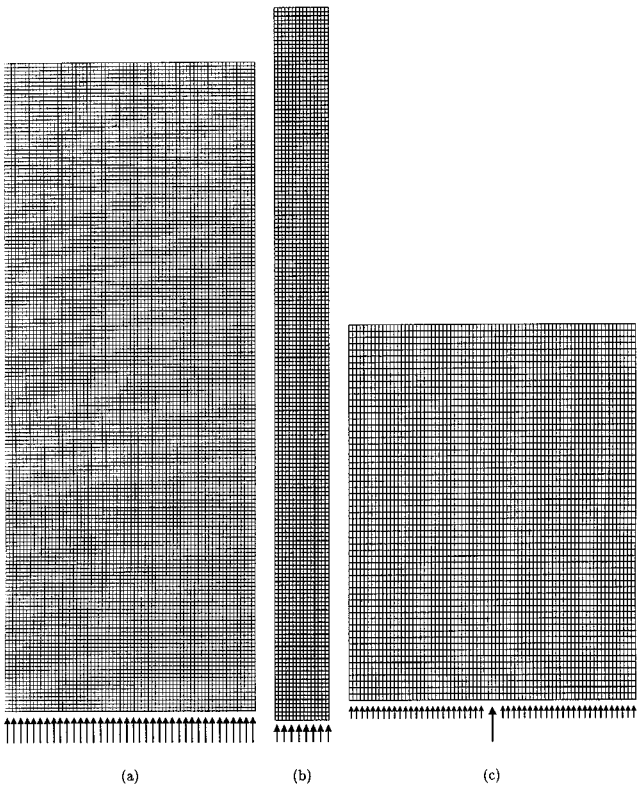

Figure 7. Computational grid of simulated fluidized beds with the gas inlet boundary condition.

(*a*) Freely bubbling fluidized bed; (b) slugging fluidized bed, (c) bubble injection into a fluidized bed.

herent instability of the gas–solid system. The behavior of the bubbles significantly affects the flow phenomena in the fluidized bed, that is, solid mixing, entrainment, and heat and mass transfer. The test cases in this comparative study are used to investigate the effect of different closure models and governing equations on the bubble behavior and bed expansion. Simulation results of each test case are compared to generally accepted experimental data and (semi)empirical models. The system properties and computational parameters for each of the test cases are given in Table 7; the computational meshes are also shown in Figure 7. The test cases are discussed in greater detail in the following sections.

Freely bubbling fluidized beds

In the freely fluidized-bed case, the gas flow is distributed uniformly across the inlet of the bed. Small bubbles form at the bottom of the fluidized bed that rise, coalesce, and erupt as large bubbles at the fluidized-bed surface. In order to evaluate model predictions, we use the Darton et al. (1977) bubble model for bubble growth in freely bubbling fluidized beds. This model is based upon preferred paths of bubbles where the distance traveled by two neighboring bubbles before coalescence is proportional to their lateral separation. Darton et al. (1977) have validated their model with measurements of many researchers. Their proposed bubble-growth equation for Geldart type *B* particles is

$$D_b = 0.54\left(U - U_{mf}\right)^{0.4}\left(h + 4\sqrt{A_0}\right)^{0.8} g^{-0.2}, \qquad (38)$$

where D_b is the bubble diameter, h is the height of the bubble above the inlet of the fluidized bed, U is the actual superficial gas inlet velocity, and A_0 is the ''catchment area'' that characterizes the distributor. For a porous-plate gas distributor, Darton et al. (1977) propose $4\sqrt{A_0} = 0.03$ m.

Werther and Molerus (1973) have developed a small capacitance probe and the statistical theory to measure the bubble diameter and the bubble rise velocity in fluidized beds using this probe. This capacitance probe can be placed in the fluidized bed at different heights and radial positions in the bed. The bubble rise velocity is determined by placing two vertically spaced probes and correlating the obtained data. The capacitance probe measures the bubbles passing it, that is, the bubble is pierced by the capacitance probe. The duration of this piercing is dependent upon the size of the bubble, the rise velocity of the bubble, and the vertical position of the bubble relative to the probe.

Hilligardt and Werther (1986) have done many measurements of bubble size and bubble velocity under various conditions using the probe developed by Werther and Molerus (1973) and have correlated their data in the form of the Davidson and Harrison (1963) bubble model. Hilligardt and

Table 7. System Properties and Computational Parameters

Parameter	Description	Freely Bubbling Fluidized Bed	Slugging Fluidized Bed	Bubble Injection into Fluidized Bed (Kuipers, 1990)
ρ_s [kg/m^3]	Solid density	2,640	2,640	2,660
ρ_g [kg/m^3]	Gas density	1.28	1.28	1.28
μ_g [Pa·s]	Gas viscosity	1.7×10^{-5}	1.7×10^{-5}	1.7×10^{-5}
d_s [μm]	Particle diameter	480	480	500
e	Coefficient of restitution	0.9	0.9	0.9
$\epsilon_{\max}$	Max. solid volume fraction	0.65	0.65	0.65
U_{mf} [m/s]	Minimum fluidization velocity	0.21	0.21	0.25
D_T [m]	Inner column diameter	0.5	0.1	0.57
H_t [m]	Column height	1.3	1.3	0.75
H_{mf} [m]	Height at minimum fluidization	0.97	0.97	0.5
$\epsilon_{s,mf}$	Solids volume fraction at minimum fluidization	0.42	0.42	0.402
Δx [m]	x-mesh spacing	7.14×10^{-3}	6.67×10^{-3}	7.50×10^{-3}
Δy [m]	y-mesh spacing	7.56×10^{-3}	7.43×10^{-3}	1.25×10^{-2}

Werther propose a variant of the Davidson and Harrison (1963) model for predicting the bubble rise velocity as a function of the bubble diameter,

$$u_b = \psi\left(U - U_{mf}\right) + \varphi\nu\sqrt{gd_b}\,, \tag{39}$$

where φ is the analytically determined square root of the Froude number of a single rising bubble in an infinitely large homogeneous area. Pyle and Harrison (1967) have determined that $\varphi = 0.48$ for a two-dimensional geometry, whereas in three dimensions the Davies-Taylor relationship gives $\varphi = 0.71$. The symbols ψ and ν, added by Hilligardt and Werther (1986), are empirical coefficients based on their data, which are dependent upon the type of particles and the width and height of the fluidized bed. For the particles and geometry employed in this study, Hilligardt and Werther (1986) propose $\psi \approx 0.3$ and $\nu \approx 0.8$. Proposals of values for ψ and ν under various fluidization conditions, determined by simulations, are given by Van Wachem et al. (1998).

Hilligardt and Werther (1986) also measured bed expansion under various conditions. Predictions of the bed expansion from the simulations are compared to these data.

Slugging fluidized beds

In the case of the slugging fluidized beds, coalescing bubbles eventually reach a diameter of 70% or more of the column diameter, resulting from either a large inlet gas velocity or a narrow bed. The operating conditions employed in the simulations correspond to the slugging conditions reported by Kehoe and Davidson (1971), who present a detailed study of slug flow in fluidized beds. The experiments of Kehoe and Davidson (1971) were performed in slugging fluidized beds of 2.5-, 5-, and 10-cm diameter columns using Geldart B particles from 50-μm to 300-μm diameter and with superficial gas inlet velocities of up to 0.5 m/s. X-Ray photography was used to determine the rise velocity of slugs and to determine the bed expansion. Kehoe and Davidson (1971) use their data to validate two different equations for the slug rise velocity, both based on two-phase theory:

$$u_{\text{slug}} = U - U_{mf} + \frac{\varphi}{2}\sqrt{gD_T} \tag{40}$$

$$u_{\text{slug}} = U - U_{mf} + \frac{\varphi}{2}\sqrt{2\,gD_T}\,, \tag{41}$$

where φ is the analytically determined square root of the Froude number of a single rising bubble. Equation 40 is the exact two-phase theory solution, and Eq. 41 is a modification of Eq. 40, based on the following observations:

1. For fine particles (< 70 μm) the slugs travel symmetrically up in the fluidized bed, so the slug rise velocity is increased by coalescence.

2. For coarser particles (> 70 μm) the slugs tend to move up the walls, which also increases their velocity.

According to Kehoe and Davidson (1971), Eqs. 40 and 41 give upper and lower bounds on the slug rise velocity. Furthermore, Kehoe and Davidson (1971) measured the maximum bed expansion ($H_{\max}$) during slug flow. They validated their theoretical analysis, which led to the result that

$$\frac{H_{\max} - H_{mf}}{H_{mf}} = \frac{U - U_{mf}}{u_{\text{bub}}}, \tag{42}$$

where u_{bub} is the rise velocity of a slug without influence of the gas phase,

$$u_{\text{bub}} = \frac{\varphi}{2}\sqrt{gD_T} \tag{43}$$

or

$$u_{\text{bub}} = \frac{\varphi}{2}\sqrt{2\,gD_T}\,, \tag{44}$$

corresponding to Eqs. 40 and 41. Hence, they also propose upper and lower bounds on the maximum bed expansion.

Bubble injection in fluidized beds

Single jets entering a minimum fluidized bed through a narrow single orifice provide details of bubble formation and growth. Such experiments were carried out by Kuipers (1990). Kuipers (1990) reported the shape of the injected bubble as well as the quantitative size and growth of the bubble with time using high-speed photography. The superficial gas-inlet velocity from the orifice was $U = 10$ m/s, and the orifice was $d = 1.5 \times 10^{-2}$ m wide.

Results and Discussion

Predictions based on simulations of these three test cases are used to compare the different governing and closure models. For this comparative study, only one particular closure model is varied at a time, to determine the sensitivity of the model predictions to that particular closure. No coupling effects were investigated. The default governing equations are those given by Jackson (1997), and the default closure models are the solid-phase stress of Hrenya and Sinclair (1997), the radial distribution function of Lun and Savage (1986), the frictional model of Johnson and Jackson (1987) with empirical values given by Johnson et al. (1990), the complete granular energy balance neglecting J_s, and the drag coefficient model of Wen and Yu (1966). For animations of some of the simulations, please refer to our Website http://www.tcp.chem.tue.nl/~scr/wachem/compare.html.

Governing equations

Simulations of the slugging bed case were performed with both the Ishii (1975) and the Jackson (1997) governing equations. Figure 8 shows the predicted maximum bed expansion with increasing gas velocity during the slug flow and the two correlations of Kehoe and Davidson (1971). Figure 9 shows the increasing slug rise velocity with increasing gas velocity. Clearly, the exact formulation of the governing equation does not have any significant influence on the prediction of these macroscopic engineering quantities, and both CFD models do a good job at predicting these quantities. Microscopically, however, there does seem to be a difference in the predic-

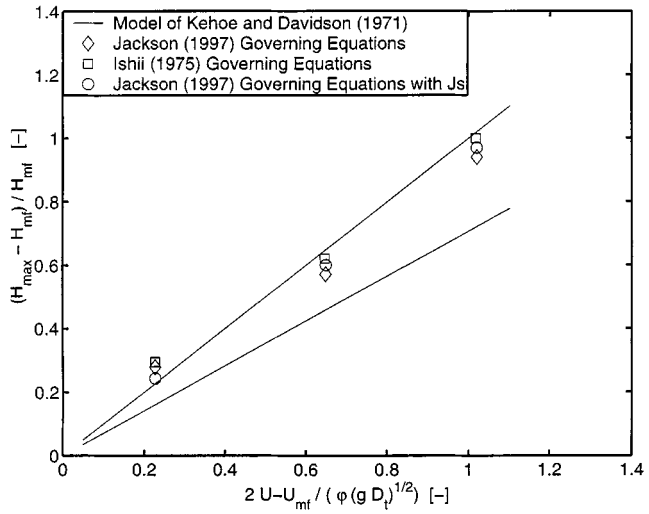

Figure 8. Predicted maximum expansion of a slugging fluidized bed with increasing gas velocity with the governing equations of Jackson (1997) and Ishii (1975), and the additional term J_s in the granular energy equation.

The predictions are compared with the two-phase theory as proposed and validated by Kehoe and Davidson (1971).

tions, as indicated in Figure 10. The flow of the gas phase in areas of large solid volume-fraction gradient is slightly different, leading to a different solids distribution. Specifically, Figure 10 shows that the Jackson (1997) governing equations produce a more round-nosed bubble shape than the Ishii (1975) equations, because the path of the gas phase is different.

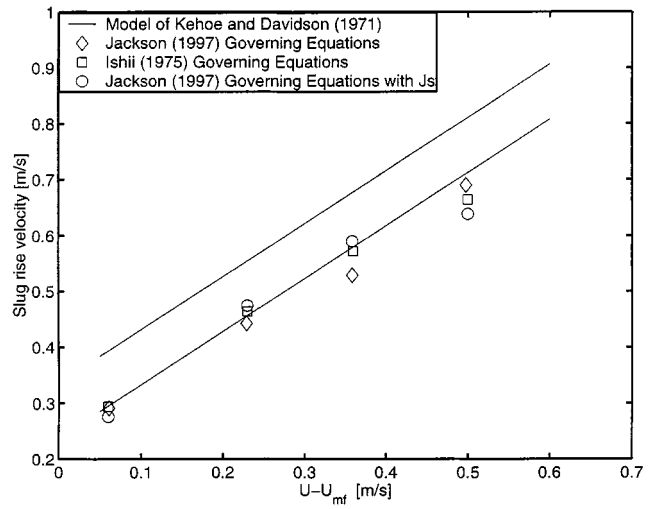

Figure 9. Predicted slug rise velocity with increasing gas velocity with the governing equations of Jackson (1997) and Ishii (1975), and the additional term J_s in the granular energy equation.

The predictions are compared with the two-phase theory as proposed and validated by Kehoe and Davidson (1971). The constant $\varphi = 0.48$.

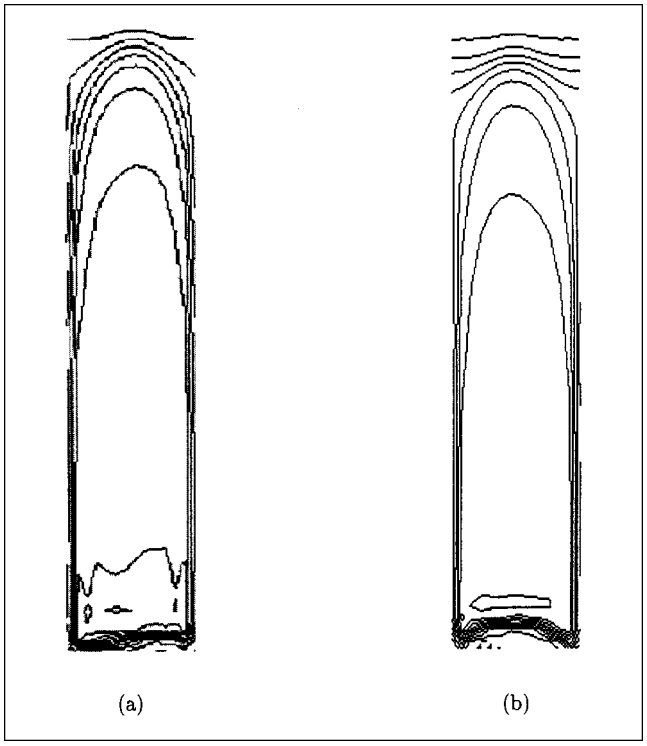

Figure 10. Rising bubble in a slugging fluidized bed predicted by (a) employing the governing equations of Jackson (1997), and by (b) employing the governing equations of Ishii (1975) at the same real time; the lines are contours of equal solid volume fraction.

Solids stress models

The exact solid-phase stress description does not influence either the freely bubbling or the slugging fluidized-bed predictions, as is expected from Figure 1; this figure shows that between 0.4 and 0.6 solids volume fraction, which is dominant in the cases studied, all solids-phase stress predictions are equal. Moreover, the influence of the radial distribution upon the stress does not give rise to any variation in the predictions of the engineering quantities associated with these simulations; the variation of the solids phase stress as a function of radial distribution function, shown in Figure 4, is small between 0.4 and 0.6 solids volume fraction, as long as the Carnahan and Starling (1969) equation is not employed. From the magnitude of the terms on the solid-phase momentum balance during simulations of fluidized beds, it can be concluded that gravity and drag are the dominating terms and that solids-phase stress predicted by kinetic theory plays a minor role.

Drag models

Coordinating with results of the comparison of the drag models shown in Figure 6, the Syamlal et al. (1993) drag leads to a lower predicted pressure drop and lower predicted bed expansion than the other two drag models. Figure 11 shows the average simulated bed expansion employing different drag

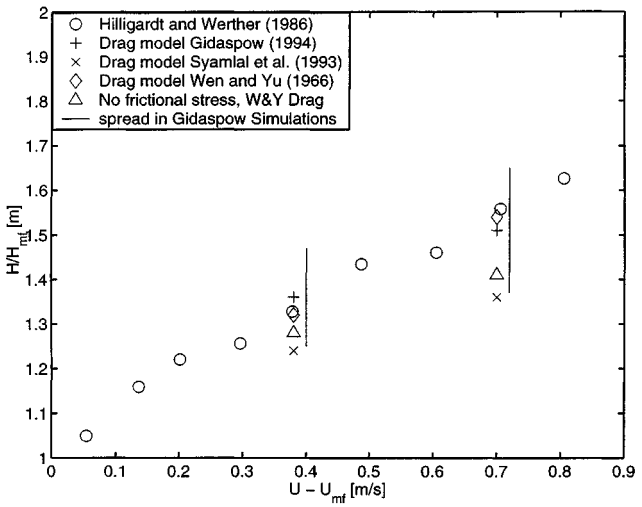

Figure 11. Predicted bed expansion as a function of gas velocity based on different drag models and with and without frictional stress.

The predictions are compared to the experimental data of Hilligardt and Werther (1986). The spread in the simulation data with the drag model of Gidaspow (1994) is indicated by the line.

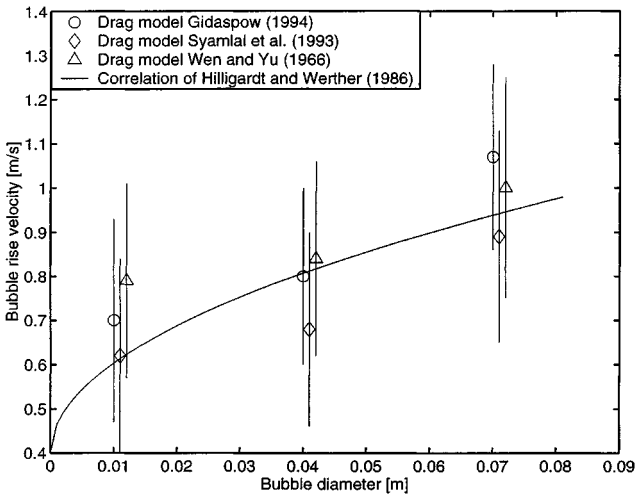

Figure 13. Predicted bubble rise velocity as a function of the bubble diameter at $U = 0.54$ m/s based on different drag models and compared to the experimental correlation of Hilligardt and Werther (1986).

The vertical lines indicate the spread of the simulated bubble rise velocity.

models in the freely bubbling fluidized-bed case, compared to measurements of Hilligardt and Werther (1986). The drag model of Syamlal et al. (1993) underpredicts the bed expansion compared to the findings of Hilligardt and Werther (1986), and therefore also underpredicts the gas holdup in the fluidized bed.

Figure 12 shows the simulated bubble size as a function of the bed height when employing different drag models, compared with the Darton et al., (1977) equation. Although the spread in the simulations is fairly large, all of the investigated drag models are in agreement with the equation put forth by Darton et al. (1977). Figure 13 shows the predicted bubble rise velocity employing different drag models in a freely bubbling fluidized bed, compared to the empirical correlation of Hilligardt and Werther (1986). All of the investigated drag models are in fairly good agreement with the empirical correlation.

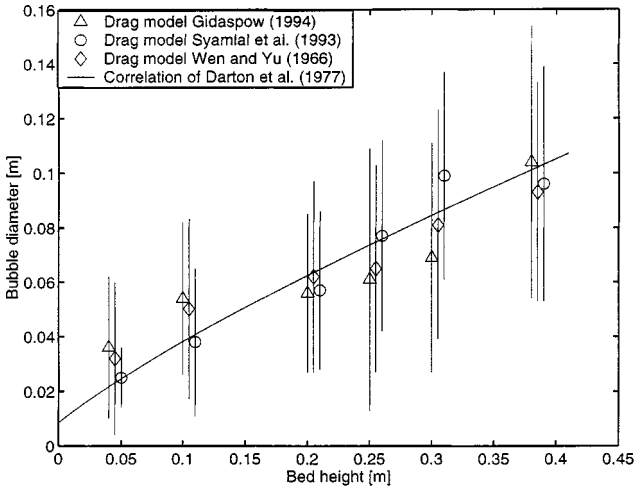

Figure 12. Predicted bubble size as a function of bed height at $U = 0.54$ m/s based on different drag models and compared to the correlation of Darton et al. (1977).

The vertical lines indicate the spread of the simulated bubble size.

Because the bubble sizes predicted by the different drag models are all close, while the predicted bed expansion differs between the models, variations in the predicted solid-volume fraction of the dense phase exist between the models, with the Syamlal et al. (1993) drag model predicting the highest solid volume fraction in the dense phase.

Figure 14 shows the quantitative bubble-size prediction for a single jet entering a minimum fluidized bed based on the drag models of Wen and Yu (1966) and Syamlal et al. (1993), which are compared to the experimental data of Kuipers (1990). Moreover, in Figure 15 we show the resulting qualitative predictions of the bubble growth and shape, and also compare these with photographs by Kuipers (1990). The Wen and Yu (1966) drag model yields better agreement with Kuipers' (1990) findings for both the bubble shape and size than the Syamlal et al. (1993) drag model. The Syamlal et al. (1993) drag model underpredicts the bubble size and produces a bubble that is more circular in shape than in the experiments of Kuipers (1990) and in the simulations with the Wen and Yu (1966) drag model.

Frictional stress

Frictional stresses can increase the total solid-phase stress by orders of magnitude, and is an important contributing force in dense gas–solid modeling. The simulation of the single jet

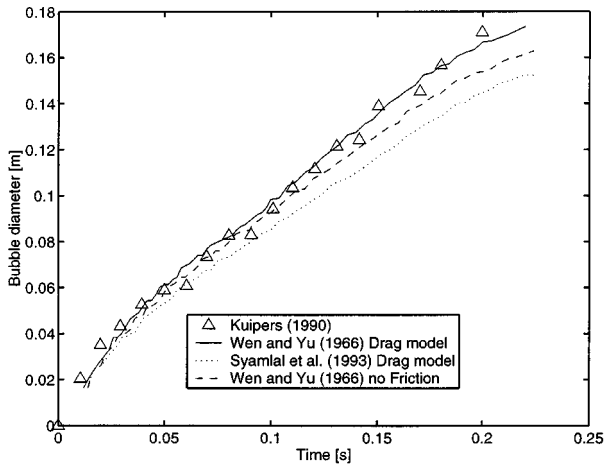

Figure 14. Bubble diameter as a function of time for a bubble formed at a single jet of $U = 10$ m/s.

A comparison is made between the experiments of Kuipers (1990), model simulations using the drag coefficient of Wen and Yu (1966) with and without frictional stress, and model simulations using the interphase drag constant of Syamlal et al. (1993).

entering a fluidized bed reveals that the size of the bubble is not significantly influenced by the frictional stress, as shown in Figure 14. However, Figure 11 shows that the predicted bed expansion in the freely bubbling fluidized bed is significantly less without frictional stress. Moreover, the number of iterations for obtaining a converged solution is almost doubled when frictional stress is omitted. Without frictional stress, there is less air in the dense phase, the maximum achieved solids packing is higher (maximum achieved solids volume fraction increased from 0.630 to 0.649), and the bed expansion is less. Moreover, the solid-phase stress in the dense regions are significantly decreased because the predicted granular temperature in the dense region of flow is very low ($\Theta \approx 10^{-5} \mathrm{m^2 \cdot s^{-2}}$) due to the magnitude of the dissipation term. When frictional stress is neglected in the simulations, convergence difficulty arises because the maximum solid volume fraction specified in the radial distribution function is approached and the derivative of the radial distribution function near maximum solid volume fraction is extremely steep. In order to still obtain convergence, we have written the radial distribution function as a Taylor series approximation at very high solid volume fraction. Adding frictional stress in the simulations prevents this problem, because then the solid volume fraction does not approach the maximum packing value.

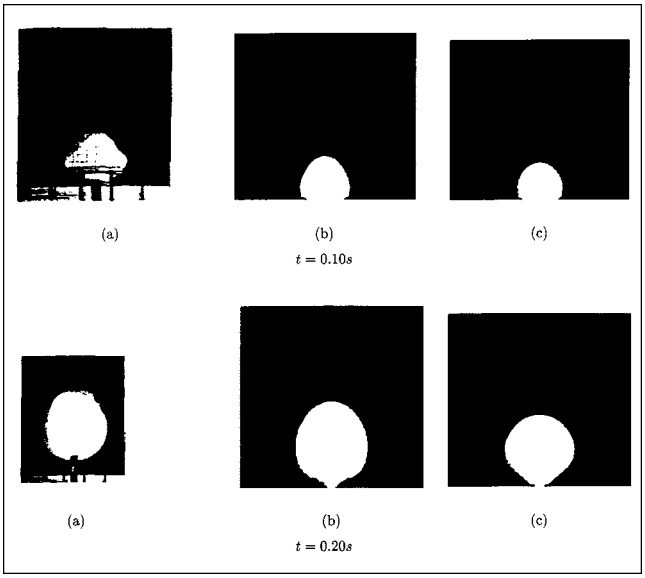

Figure 15. Experimental and simulated bubble shape associated with a single jet at $U = 10$ m/s and at $t = 0.10$ s and $t = 0.20$ s.

Comparison is made between the (a) experiment of Kuipers (1990); (b) model simulation using the interphase drag constant of Wen and Yu (1966); (c) model simulation using the interphase drag constant of Syamlal et al. (1993).

Granular energy balance

The influence of the additional generation and dissipation term J_s in the granular energy balance is determined in the case of the slugging fluidized bed. Figure 8 shows the predictions of the maximum bed expansion as a function of increasing gas velocity for simulations with and without this additional term. Figure 9 also shows the predicted rise velocity of the slugs with and without this additional term J_s. Although this additional term J_s results in as much as 20% higher granular temperature values (granular temperature increased from 0.138 $\mathrm{m^2 \cdot s^{-2}}$ to 0.165 $\mathrm{m^2 \cdot s^{-2}}$), this does not seem to influence the predicted bed expansion or the slug rise velocity. The exact formulation of J_s (Eq. 26 or 27) does not play a role in the predicted granular temperature.

Simulations of slugging fluidized beds were also performed using the simplified algebraic granular energy equation, Eq. 21. There were no differences in predicted bed expansion, bubble size, or bubble rise velocity due to this simplification vs. using the full granular energy balance. This simplified equation gives rise to deviations from full granular energy-balance predictions of as much as 10% in the granular temperature (granular temperature decreased from 0.138 $\mathrm{m^2 \cdot s^{-2}}$ to 0.0127 $\mathrm{m^2 \cdot s^{-2}}$). The computational effort for solving the complete granular energy equation is about 20% higher than calculating the granular temperature from the algebraic equation. More simulation results of the freely bubbling fluidized bed case with the algebraic equation are given in van Wachem et al. (1998).

Conclusions

In this article we have compared different formulations that are employed in CFD models for gas–solid flow in the Eulerian/Eulerian framework. We discussed the basis for the formulation of the two different sets of governing equations common to the two-fluid literature with respect to the nature of the dispersed phase. It is shown in detail that the modeling of gas–solid flows requires different governing equations than the modeling of gas–liquid flows. We also have compared various closure models both quantitatively and qualitatively. For example, we have shown how the hybrid drag model proposed by Gidaspow (1994) produces a discontinuity in the

drag coefficient, how an order-of-magnitude difference in the normal stress is predicted by the various frictional stress models, and how the Syamlal et al. (1993) model predicts a lower bed expansion than with the other drag models.

Finally, we have studied the impact of the two governing equations and the various closure models on simulation predictions in three fluidized-bed test cases. It is shown that the resulting predictions based on the two sets of governing equations are similar on an engineering scale, but are different in terms of microscopic features associated with individual bubbles or localized solids distributions. It is also shown that the model predictions are not sensitive to the use of different solids stress models or radial distribution functions. In dense-phase gas–solid flow, the different approaches in the kinetic theory modeling predict similar values for the solid-phase properties. From an analysis of the individual terms on the momentum balance of the solid-phase momentum balance during the simulations, it can be concluded that gravity and drag are the most dominating terms; this is why the two different sets of governing equations predict similar results, and why the exact solid-phase stress prediction is of minor importance. At a very high volume fraction, frictional stress can influence the hydrodynamic prediction due to its large magnitude. Simplifying the granular energy balance by retaining only the generation and dissipation terms is a reasonable assumption in the case of fluidized-bed modeling and reduces the computational effort by about 20%. Finally, the manner in which the drag force is modeled has a significant impact on the simulation results, influencing the predicted bed expansion and the solids concentration in the dense-phase regions of the bed.

Acknowledgments

The investigations were supported (in part) by the Netherlands Foundation for Chemical Research (SON), with financial aid from the Netherlands Organization for Scientific Research (NWO). This support is largely acknowledged. B.G.M. van Wachem gratefully acknowledges the financial support of the Netherlands Organization for Scientific Research (NWO), the Stimulation fund for Internationalization (SIR), DelftChemTech, the Delft University Fund, and the Reactor Research Foundation (RR), for the expenses for visiting Purdue University.

Notation

A = empirical constant
A_0 = catchment area of distributor, m^2
C_D = drag coefficient
d_s = particle diameter, m
$\overline{\overline{D}}_s$ = strain rate tensor, s^{-1}
D = diameter, m
D_T = inner column diameter, m
e = coefficient of restitution
f = fluid-phase point property
Fr = empirical material constant, $N \cdot m^{-2}$
$g(r)$ = weighting function
g = gravitational constant, $m \cdot s^{-2}$
g_0 = radial distribution function
h = height of bubble in fluidized bed, m
H_{mf} = minimum fluidization bed height, m
H_t = column height, m
J = fluctuating velocity/force correlation, $kg \cdot m^{-3} \cdot s^{-1}$
L = interfacial area per unit volume, m^{-1}
M = interphase momentum exchange, $N \cdot s^{-1}$
n = empirical constant in frictional stress
n = number density
$\boldsymbol{n}$ = normal vector, m
p = empirical constant in frictional stress
P = pressure, $N \cdot m^{-2}$
r = point in space, m
R = characteristic length scale, m
Re = Reynolds number
S = surface, m^2
t = time, s
U = inlet (superficial) gas velocity, $m \cdot s^{-1}$
U_{mf} = minimum fluidization velocity, $m \cdot s^{-1}$
$\boldsymbol{v}$ = velocity vector, $m \cdot s^{-1}$
V = volume, m^3
V_r = ratio of terminal velocity of a group of particles to that of an isolated particle
$\boldsymbol{x}$ = position vector, m
X = phase indicator
Δx = x-mesh spacing, m
Δy = y-mesh spacing, m

Greek letters

β = interphase drag constant, $kg \cdot m^{-3} \cdot s^{-1}$
ϵ = volume fraction
η = $1/2\ (1 + e)$
ϕ = angle of internal friction
φ = square root of the Froude number
φ' = specularity coefficient
γ = dissipation of granular energy, $kg \cdot m^{-3} \cdot s^{-1}$
κ = solids thermal conductivity, $kg \cdot m^{-1} \cdot s^{-1}$
λ = solids bulk viscosity, $Pa \cdot s$
λ_{mfp} = mean free path, m
μ = solids shear viscosity, $Pa \cdot s$
ν = empirical coefficient
ψ = empirical coefficient
ρ = density, $kg \cdot m^{-3}$
$\overline{\overline{\sigma}}$ = total stress tensor, $N \cdot m^{-2}$
$\overline{\overline{\tau}}$ = viscous stress tensor, $N \cdot m^{-2}$
Θ = granular temperature, $m^2 \cdot s^{-2}$

Subscripts

b = bubble
bub = single bubble
dil = dilute
f = frictional
g = gas phase
i = interface
k = either phase
mf = minimum fluidization
min = minimum; kick-in value
max = maximum
p = particle
s = solids phase
slip = slip
slug = slug
w = wall

Literature Cited

Alder, B. J., and T. E. Wainwright, "Studies in Molecular Dynamics: II. Behaviour of a Small Number of Elastic Spheres," *J. Chem. Phys.*, **33**, 1439 (1960).

Anderson, T. B., and R. Jackson, "A Fluid Mechanical Description of Fluidized Beds," *Ind. Eng. Chem. Fundam.*, **6**, 527 (1967).

Barthod, D., M. Del Pozo, and C. Mirgain, "CFD-Aided Design Improves FCC Performance," *Oil Gas J.*, 66 (1999).

Boemer, A., H. Qi, U. Renz, S. Vasquez, and F. Boysan, "Eulerian Computation of Fluidized Bed Hydrodynamics—A Comparison of Physical Models," *Proc. of the Int. Conf. on FBC*, Orlando, FL, p. 775 (1995).

Carnahan, N. F., and K. E. Starling, "Equations of State for Non-Attracting Rigid Spheres," *J. Chem. Phys.*, **51**, 635 (1969).

Chapman, S., and T. G. Cowling, *The Mathematical Theory of Non-Uniform Gases*, Cambridge Univ. Press, 3rd Ed., Cambridge (1970).

Coulomb, C. A., ''Essai sur Une Application des Régles de Maximis et Minimis à Quelques Problèmes de Statique, Relatifs á l'Architecture,'' *Acad. R. Sci. Mèm. Math, Phys. Divers. Savants*, **7**, 343 (1776).
Dalla Valle, J. M., *Micromeritics*, Pitman, London (1948).
Darton, R. C., R. D. LaNauze, J. F. Davidson, and D. Harrison, ''Bubble Growth Due to Coalescence in Fluidized Beds,'' *Trans. Inst. Chem. Eng.*, **55**, 274 (1977).
Davidson, J. F., and D. Harrison, *Fluidized Particles*, Cambridge Univ. Press, Cambridge (1963).
Enwald, H., E. Peirano, and A. E. Almstedt, ''Eulerian Two-Phase Flow Theory Applied to Fluidization,'' *Int. J. Multiphase Flow*, **22**, 21 (1996).
Ergun, S., ''Fluid Flow through Packed Columns,'' *Chem. Eng. Prog.*, **48**, 89 (1952).
Garside, J., and M. R. Al-Dibouni, ''Velocity-Voidage Relationship for Fluidization and Sedimentation,'' *Ind. Eng. Chem. Proc. Des. Dev.*, **16**, 206 (1977).
Gidaspow, D., *Multiphase Flow and Fluidization*, Academic Press, San Diego (1994).
Gidaspow, D., and L. Huilin, ''Equation of State and Radial Distribution Functions of FCC Particles in a CFB,'' *AIChE J.*, **44**, 279 (1998).
Hilligardt, K., and J. Werther, ''Local Bubble Gas Hold-Up and Expansion of Gas/Solid Fluidized Beds,'' *Ger. Chem. Eng.*, **9**, 215 (1986).
Hoomans, B. P. B., J. A. M. Kuipers, W. J. Briels, and W. P. M. van Swaaij, ''Discrete Particle Simulation of Bubble and Slug Formation in a Two-Dimensional Gas-Fluidised Bed: A Hard-Sphere Approach,'' *Chem. Eng. Sci.*, **51**, 99 (1996).
Hrenya, C. M., and J. L. Sinclair, ''Effects of Particle-Phase Turbulence in Gas-Solid Flows,'' *AIChE J.*, **43**, 853 (1997).
Ishii, M., *Thermo-Fluid Dynamic Theory of Two-Phase Flow*, Direction des Etudes et Recherches d'Electricité de France, Eyrolles, Paris (1975).
Ishii, M., and K. Mishima, ''Two-Fluid Model and Hydrodynamic Constitutive Relations,'' *Nucl. Eng. Des.*, **82**, 107 (1984).
Jackson, R., ''The Mechanics of Fluidized Beds: Part I: The Stability of the State of Uniform Fluidization,'' *Trans. Inst. Chem. Eng.*, **41**, 13 (1963).
Jackson, R., ''Locally Averaged Equations of Motion for a Mixture of Identical Spherical Particles and a Newtonian Fluid,'' *Chem. Eng. Sci.*, **52**, 2457 (1997).
Jackson, R., ''Erratum,'' *Chem. Eng. Sci.*, **53**, 1955 (1998).
Jenkins, J. T., ''Boundary Conditions for Rapid Granular Flow: Flat, Frictional Walls,'' *J. Appl. Mech.*, **59**, 120 (1992).
Jenkins, J. T., and S. B. Savage, ''A Theory for the Rapid Flow of Identical Smooth, Nearly Elastic, Spherical Particles,'' *J. Fluid Mech.*, **130**, 187 (1983).
Johnson, P. C., and R. Jackson, ''Frictional-Collisional Constitutive Relations for Granular Materials, with Application to Plane Shearing,'' *J. Fluid Mech.*, **176**, 67 (1987).
Johnson, P. C., P. Nott, and R. Jackson, ''Frictional-Collisional Equations of Motion for Particulate Flows and Their Application to Chutes,'' *J. Fluid Mech.*, **210**, 501 (1990).
Kehoe, P. W. K., and J. F. Davidson, ''Continuously Slugging Fluidised Beds,'' *Inst. Chem. Eng. Symp. Ser.*, **33**, 97 (1971).
Koch, D. L., ''Kinetic Theory for a Monodisperse Gas-Solid Suspension,'' *Phys. Fluids A*, **2**, 1711 (1990).
Koch, D. L., and A. S. Sangani, ''Particle Pressure and Marginal Stability Limits for a Homogeneous Monodisperse Gas-Fluidized Bed: Kinetic Theory and Numerical Simulation,'' *J. Fluid Mech.*, **400**, 229 (1999).
Kuipers, J. A. M., *A Two-Fluid Micro Balance Model of Fluidized Beds*, PhD Thesis, Univ. of Twente, Twente, The Netherlands (1990).
Louge, M. Y., E. Mastorakos, and J. T. Jenkins, ''The Role of Particle Collisions in Pneumatic Transport,'' *J. Fluid Mech.*, **231**, 345 (1991).
Lun, C. K. K., and S. B. Savage, ''The Effects of an Impact Velocity Dependent Coefficient of Restitution on Stresses Developed by Sheared Granular Materials,'' *Acta Mech.*, **63**, 15 (1986).
Lun, C. K. K., S. B. Savage, D. J. Jefferey, and N. Chepurniy, ''Kinetic Theories for Granular Flow: Inelastic Particles in Couette Flow and Slightly Inelastic Particles in a General Flowfield,'' *J. Fluid Mech.*, **140**, 223 (1984).
Nadim, A., and H. A. Stone, ''The Motion of Small Particles and Droplets in Quadratic Flows,'' *Stud. Appl. Mech.*, **85**, 53 (1991).
Ocone, R., S. Sundaresan, and R. Jackson, ''Gas-Particle Flow in a Duct of Arbitrary Inclination with Particle-Particle Interactions,'' *AIChE J.*, **39**, 1261 (1993).
Patankar, S. V., *Numerical Heat Transfer and Fluid Flow*, Hemisphere, New York (1980).
Pyle, D. L., and D. Harrison, *Chem. Eng. Sci.*, **22**, 531 (1967).
Rhie, C. M., and W. L. Chow, ''Numerical Study of the Turbulent Flow Past an Airfoil with Trailing Edge Separation,'' *AIAA J1*, **21**, 1527 (1983).
Richardson, J. F., and W. N. Zaki, ''Sedimentation and Fluidisation: I,'' *Trans. Inst. Chem. Eng.*, **32**, 35 (1954).
Rowe, P. N. ''Drag Forces in a Hydraulic Model of a Fluidized Bed: II,'' *Trans. Inst. Chem. Eng.*, **39**, 175 (1961).
Sangani, A. S., G. Mo, H.-K. Tsao, and D. L. Koch, ''Simple Shear Flows of Dense Gas-Solid Suspensions at Finite Stokes Numbers,'' *J. Fluid Mech.*, **313**, 309 (1996).
Schaeffer, D. G., ''Instability in the Evolution Equations Describing Incompressible Granular Flow,'' *J. Differ. Eqs.*, **66**, 19 (1987).
Sinclair, J. L., ''Hydrodynamic Modelling,'' *Circulating Fluidized Beds*, J. R. Grace, A. A. Evidan, and T. M. Knowlton, eds., Blackie, London, p. 149 (1997).
Sinclair, J. L., and R. Jackson, ''Gas-Particle Flow in a Vertical Pipe with Particle-Particle Interactions,'' *AIChE J.*, **35**, 1473 (1989).
Syamlal, M., W. Rogers, and T. J. O'Brien, ''Mfix Documentation Theory Guide,'' U.S. Dept. of Energy, Office of Fossil Energy, Tech. Note (1993).
Tsuji, Y., T. Kawaguchi, and T. Tanaka, ''Discrete Particle Simulation of Two-Dimensional Fluidized Bed,'' *Powder Technol.*, **77**, 79 (1993).
Van Wachem, B. G. M., J. C. Schouten, R. Krishna, and C. M. van den Bleek, ''Eulerian Simulations of Bubbling Behaviour in Gas-Solid Fluidised Beds,'' *Comput. Chem. Eng.*, **22**, s299 (1998).
Van Wachem, B. G. M., J. C. Schouten, R. Krishna, and C. M. van den Bleek, ''Validation of the Eulerian Simulated Dynamic Behaviour of Gas-Solid Fluidised Beds,'' *Chem. Eng. Sci.*, **54**, 2141 (1999).
Wen, C. Y., and Y. H. Yu, ''Mechanics of Fluidization,'' *Chem. Eng. Prog. Symp. Ser.*, **62**, 100 (1966).
Werther, J., and O. Molerus, ''The Local Structure of Gas Fluidized Beds I. A Statistically Based Measured System,'' *Int. J. Multiphase Flow*, **1**, 103 (1973).
Zhang, D. Z., and R. M. Rauenzahn, ''A Viscoelastic Model for Dense Granular Flows,'' *J. Rheol.*, **41**, 1275 (1997).

Manuscript received Dec. 7, 1999, and revision received Oct. 9, 2000.